Catalysis Today 142 (2009) 143–151

Contents lists available at ScienceDirect

Catalysis Today

journal homepage: www.elsevier.com/locate/cattod

The role of surface vanadia species in butane dehydrogenation over VO_x/Al_2O_3

J. McGregor [a,*], Z. Huang [a], G. Shiko [a], L.F. Gladden [a], R.S. Stein [b], M.J. Duer [b], Z. Wu [c], P.C. Stair [c], S. Rugmini [d], S.D. Jackson [d]

[a] University of Cambridge, Department of Chemical Engineering, New Museums Site, Pembroke Street, Cambridge CB2 3RA, UK
[b] University of Cambridge, Department of Chemistry, Lensfield Road, Cambridge CB2 1EW, UK
[c] Department of Chemistry, Northwestern University, IL 60208, USA
[d] WestCHEM, Department of Chemistry, University of Glasgow, Glasgow G12 8QQ, UK

ARTICLE INFO

Article history:
Available online 30 August 2008

Keywords:
Vanadia catalysts
Alkane dehydrogenation
Oxidation kinetics
Solid-state NMR

ABSTRACT

A series of θ-Al_2O_3 supported VO_x catalysts, of different vanadium loadings, have been characterised and employed for the selective dehydrogenation of *n*-butane. Characterisation of the unreacted catalysts has been carried out by solid-state NMR (^{51}V MAS NMR, ^{27}Al MAS NMR and ^{27}Al 3Q-MAS NMR), and FT-IR spectroscopies, with reference to previously acquired Raman and UV–vis spectroscopy data. As vanadium loading increases, so does the domain size of the supported vanadate units with significant quantities of V_2O_5 observed at the highest loadings. The influence of calcination, pre-reduction, reaction and regeneration on the structure of the catalysts has been studied by NMR, FT-IR, EPR, microanalysis and TEOM. Calcination disperses crystalline vanadate units, and at high loadings $AlVO_4$ formation is observed. Pre-reduction reduces the vanadium oxidation state from 5+ to 3+, while regeneration results in the formation of highly crystalline V^{5+} species. From these data it is possible to determine structure–activity relationships, with polymeric vanadia clusters favouring the formation of butenes and butadienes, while more isolated species are highly active towards the formation of polynuclear aromatic hydrocarbons retained on the catalyst surface post-reaction. These large polynuclear aromatic hydrocarbons are however not the principle cause of catalyst deactivation in this reaction.

1. Introduction

The catalytic dehydrogenation and oxidative dehydrogenation (ODH) of light alkanes is an important route to the formation of alkenes and alkadienes, important precursors for fuels, plastics and many other materials. In particular, a substantial body of research has focused on supported VO_x catalysts for ODH reactions [1–6]. Such reactions are believed to proceed *via* a Mars–van Krevelen mechanism in which reduced VO_x centres that form during reaction are reoxidised by gas-phase oxygen. Recently, studies have investigated the direct dehydrogenation of light alkanes over supported VO_x catalysts in the absence of gas-phase oxygen where a different reaction mechanism must operate [7–11]. A number of studies have investigated the structure of supported VO_x units in catalysts for *n*-butane dehydrogenation [12–16]. Despite this, there remains a lack of understanding as to the distinct role played by the different surface species present on supported catalysts. In this work we attempt to redress this through characterisation of a series of θ-Al_2O_3 supported VO_x catalysts at all stages during the direct dehydrogenation of *n*-butane in the absence of gas-phase oxygen: as-prepared, calcined, reduced, post-reaction and post-regeneration. These data are then related to catalytic activity measurements providing insights into the relationship between surface VO_x species and catalytic activity and selectivity.

2. Experimental

2.1. Materials

The catalysts employed in this study are alumina-supported VO_x catalysts with nominal metal loadings of 1 wt.%, 3.5 wt.% and 8 wt.%, and their synthesis has previously been described in the literature [7–9,14]. These will henceforth be referred to as 1 V, 3.5 V and 8 V, respectively. Prior to use the catalyst extrudates were ground and sieved to a particle size of 75–90 μm.

2.2. Catalytic activity measurements

Catalytic activity data were acquired using a fixed-bed reactor connected to an on-line GC (Agilent 6890). The catalyst (1.5 cm^3)

* Corresponding author. Tel.: +44 1223 330134; fax: +44 1223 334796.
E-mail address: jm405@cam.ac.uk (J. McGregor).

0920-5861/$ – see front matter © 2008 Elsevier B.V. All rights reserved.
doi:10.1016/j.cattod.2008.07.022

was heated (5 K min^{-1}) to the calcination temperature in 5% O_2/N_2 (0.5 barg, 40 ml min^{-1}) and held at this temperature for 2 h. A flow of He (0.5 barg, 42 ml min^{-1}) was then established and the temperature adjusted to the desired reaction temperature. 3% *n*-C_4H_{10}/N_2 was then introduced (0.5 barg, 60 ml min^{-1}) for a period of 3 h. GC measurements were taken at regular intervals. After 3 h the catalyst was cooled to room temperature in flowing He and either removed for *ex situ* analysis or regenerated at 873 K. For regeneration the catalyst was heated at 5 K min^{-1}, and then held at 873 K for 3 h. Conversion and selectivity were calculated using Eqs. (1) and (2), respectively:

$$\%\,\text{Conversion} = 100 \times \left[1 - \frac{X}{Y}\right] \quad (1)$$

$$\%\,\text{Selectivity} = 100 \times \left[\frac{Z}{P}\right] \quad (2)$$

The quantity of *n*-butane fed to the reactor is denoted by *Y*, the quantity of *n*-butane at the reactor outlet is denoted by *X*, while *Z* represents the quantity of a specific reaction product. *P* is the sum of all reaction products including deposited carbon.

2.3. Catalyst characterisation techniques

The catalysts have been characterised spectroscopically by EPR, FT-IR and solid-state NMR. EPR spectra were measured on a Bruker ER-200D series EPR spectrometer at room temperature in the region 200–6200 G with a microwave frequency of 9.34 GHz (X-band). All NMR spectra were acquired on an AV-400 spectrometer (Bruker). ^{51}V and ^{27}Al MAS NMR spectra were acquired using an ordinary pulse-acquire sequence, in which the pulse width was 2 μs. Spinning speeds of 12 kHz and 14 kHz were used. The chemical shifts of ^{51}V and ^{27}Al are referenced to the ^{51}V resonance of $VOCl_3$ (0 ppm) and to the ^{27}Al resonance of aqueous $Al(NO_3)_3$ (0 ppm), respectively. For ^{27}Al 3Q-MAS measurements, the split t_1 pulse-sequence of Brown and Wimperis [17] was used, while the spinning rate was 10 kHz. ^{13}C CP-MAS NMR was conducted at a ^{13}C operating frequency of 100.65 MHz. Chemical shifts were referenced to a solid CH_2 adamantane shift at 38.54 ppm relative to tetramethylsilane. Diffuse reflectance FT-IR spectra, averaged over 4096 scans, were acquired at room temperature on an Avatar 380 (Thermo Scientific). A tapered element oscillating microbalance (TEOM 1500, R&P) has been employed to provide measurements of mass changes occurring during reduction and oxidation experiments. A detailed explanation of the operating principles of the TEOM is provided by Chen et al. [18].

3. Results and discussion

3.1. Characterisation of as-prepared catalysts

The as-prepared catalysts have been characterised by TEOM, BET surface area measurements, FT-IR, and solid-state NMR spectroscopy. Both the structure of the supported VO_x units and that of alumina support have been investigated.

The vanadia loading and BET surface areas of the catalysts are listed in Table 1. For comparison the surface area of the pure support material is 106 $m^2\,g^{-1}$. As expected, the measured surface area decreases with increasing vanadium loading, from 104 $m^2\,g^{-1}$ for 1 V to 77 $m^2\,g^{-1}$ for 8 V. In line with this decrease in surface area, FT-IR spectra reveal a corresponding loss of hydroxyl sites. Fig. 1(a) shows FT-IR spectra for the three VO_x/Al_2O_3 catalysts and the pure support. The broad band, centred at ~3500 cm^{-1}, present in all spectra corresponds to chemisorbed water. The hydroxyl groups present have characteristic vibrations from 3200 cm^{-1} to 4000 cm^{-1} and are sequentially titrated by VO_x species with the most basic hydroxyls, *i.e.* those at higher wavenumbers (*e.g.* 3750 cm^{-1}), being the first to be lost at low vanadium loadings, while less basic hydroxyls (at lower wavenumbers) are only eliminated at higher loadings. This behaviour had previously been observed by Turek et al. for a number of different Al_2O_3 supported metal oxide catalysts [19]. Inspection of the V=O stretching region (~800–1200 cm^{-1}) in Fig. 1(a) reveals that in this region the spectra are dominated by features present in the pure support spectrum. Solid-state ^{51}V MAS NMR studies reveal further insights. NMR spectra have been acquired of all the samples and are shown in Fig. 2(a), focused on the region of interest. An isotropic resonance is identified at −612 ppm in both 3.5 V and 8 V. This resonance is indicative of V^{5+} in a V_2O_5-like environment. The quantity of this species, shown by the intensity of the peak, is greater for 8 V than for 3.5 V, with no signal observed from 1 V. These data show good agreement with previous Raman spectroscopy studies [20]. Employing both UV and visible Raman spectroscopy these previous studies provided a quantitative determination of the different surface species (monomeric vanadates, polymeric vanadates and crystalline vanadia) present [20]. It was shown that monomeric vanadate species are predominant on the surface of catalysts with vanadium loadings ≤1 wt.%. As the vanadia loading increases, polyvanadate and crystalline V_2O_5 become the dominant vanadia species representing 60% and 10%, respectively of vanadium on the surface of 3.5 V. At higher loadings the fraction of V_2O_5 increases, reaching 30% on 8 V consistent with ^{51}V MAS NMR results reported herein.

In the present work, ^{27}Al MAS NMR studies have been conducted on each of the three catalysts and on the pure support. In all cases the recorded spectra contain peaks located in two distinct regions: a sharp, high intensity peak at ~6 ppm, and a broad region of lower intensity between 25 ppm and 70 ppm, illustrated in Fig. 3(a) for 8 V. The peak at ~6 ppm is characteristic of Al in a sixfold, octahedral, co-ordination while the downfield region may contain aluminium in both fivefold and fourfold (tetrahedral) co-ordinations. In addition to conventional MAS NMR spectra, ^{27}Al 3Q-MAS NMR spectra have also been acquired, as illustrated in Fig. 3(b) for 8 V. The projection of such spectra in the ^{27}Al indirect dimension (F1) yields the isotropic peaks, while the anisotropic lineshapes (corresponding to a standard MAS spectrum) are displayed by the projection in the ^{27}Al directly detected single-quantum dimension (F2). The resolution of the isotropic signals provided

Table 1
Catalyst characterisation

Catalyst (V)	V (wt.%)	BET ($m^2\,g^{-1}$) (as-prepared catalysts)	BET ($m^2\,g^{-1}$) (post-reaction)
1	0.8	104	99
3.5	3.7	94	76
8	7.9	77	32

Vanadium loadings, and BET surface area of as-prepared 1 V, 3.5 V and 8 V, and BET surface areas after regeneration at 873 K.

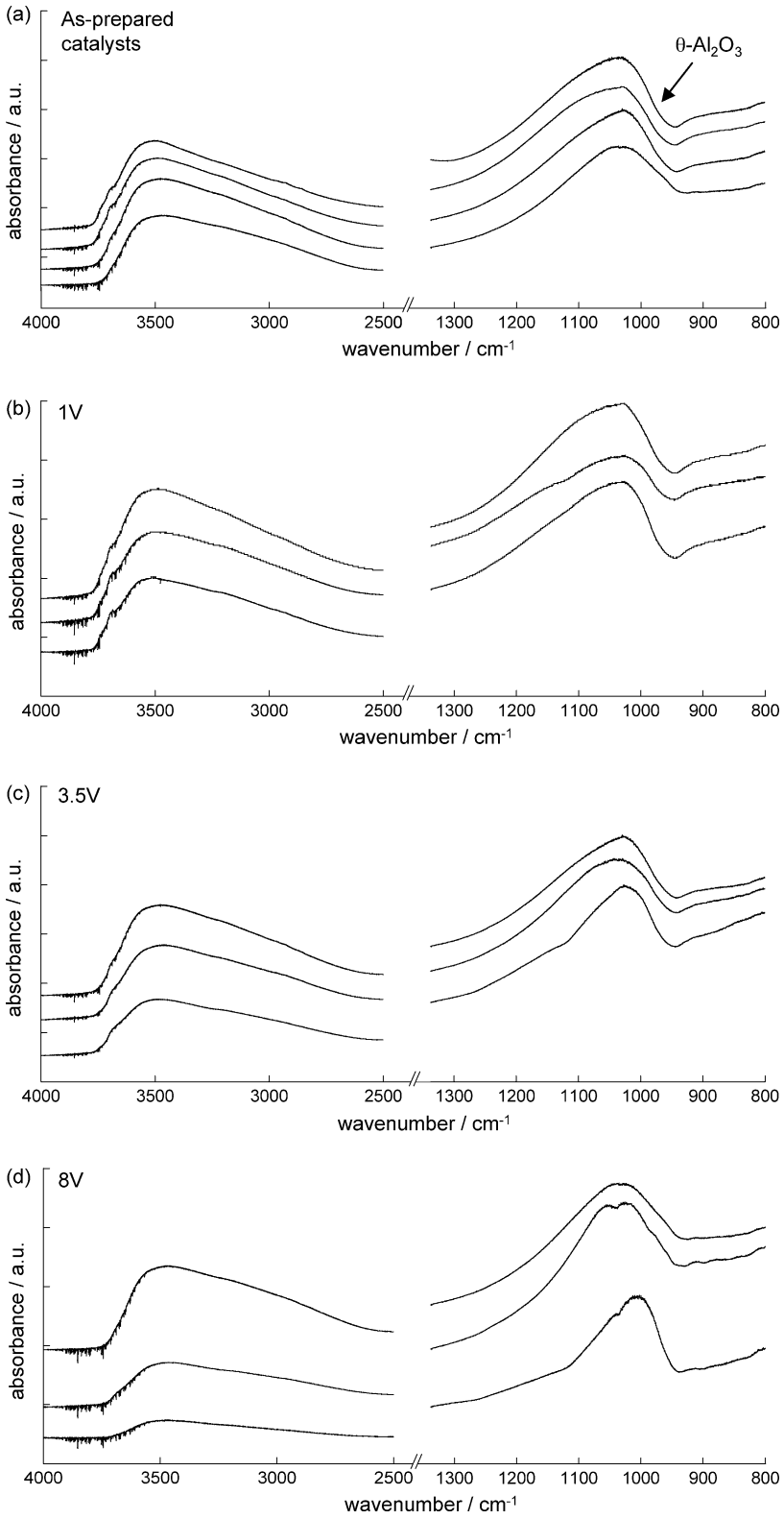

Fig. 1. FT-IR spectra of VO_x/Al_2O_3 catalysts. (a) As-prepared catalysts; from top, θ-Al_2O_3; 1 V, 3.5 V and 8 V. (b–d) 1 V, 3.5 V and 8 V, respectively; from top as-prepared, calcined at 973 K and regenerated at 873 K. Spectra are offset for clarity.

by the 3Q-MAS experiment confirms the presence of both 5- and 4-co-ordinate Al in addition to octahedral Al. The isotropic resonances of these three environments are 78.2 ppm, 73.2 ppm and 10.2 ppm.

3.2. Influence of calcination on catalyst structure

The catalysts employed in this study have been pre-calcined at 823 K. Calcination temperature is known to strongly influence

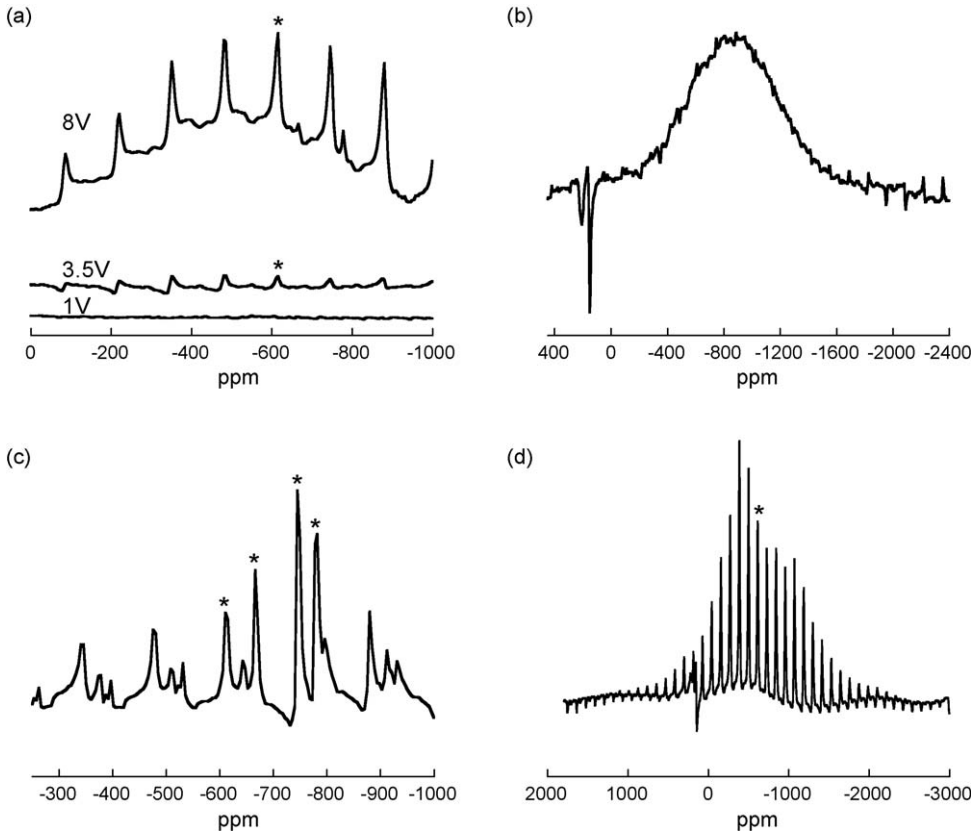

Fig. 2. ^{51}V MAS NMR spectra. (a) As-prepared catalysts, from top 8 V, 3.5 V and 1 V, (b) 3.5 V after calcination at 973 K, (c) 8 V after calcination at 973 K, and (d) 8 V after regeneration at 873 K. (*) indicates an isotropic resonance. In spectra (b) and (d) the peaks to negative intensity correspond to Al atoms in the support.

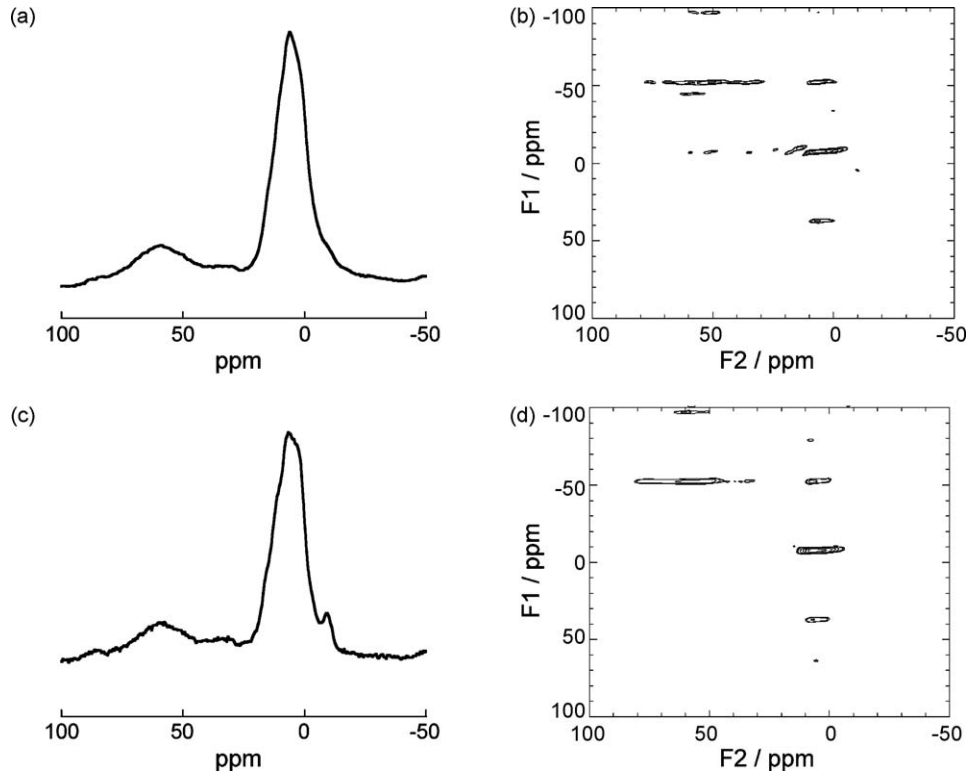

Fig. 3. ^{27}Al NMR spectra. (a) ^{27}Al MAS NMR spectrum of as-prepared 8 V, (b) ^{27}Al 3Q-MAS NMR spectrum of as-prepared 8 V, (c) ^{27}Al MAS NMR spectrum of 8 V after calcination at 973 K, and (d) ^{27}Al 3Q-MAS NMR spectrum of 8 V after regeneration at 873 K. In spectra (b) and (d) the peak at ~3 ppm in the F2 dimension has spinning sidebands in the F1 dimension.

catalyst structure and therefore catalytic performance [21,22]. Such differences can be explained by changes in the catalyst structure induced by calcination, studied herein by solid-state MAS NMR and FT-IR spectroscopy. Fig. 2(b) shows the MAS NMR spectrum of 3.5 V after calcination at 973 K. Compared to the as-prepared material the intensity of the V_2O_5 peak has reduced by 71%, while simultaneously a broad peak appears, assigned to more dispersed V^{5+} in distorted tetrahedral environments [23]. Upon increasing the catalyst loading to 8 wt.% V a similar sharp decrease in the intensity of the V_2O_5 peak (−612 ppm) occurs after calcination, with the intensity of the broad background corresponding to disordered V^{5+} species also decreasing. In addition, the formation of aluminium orthovanadate, $AlVO_4$, was observed; characterised by the appearance of peaks at −659 ppm, −757 ppm and −769 ppm [22,24] (Fig. 2(c)). Structurally, $AlVO_4$ contains three distinct, isolated, units, giving rise to the three peaks observed by ^{51}V MAS NMR [24]. The presence of $AlVO_4$ in 8 V after calcination is further confirmed through inspection of both FT-IR (Fig. 1(d)) and ^{27}Al MAS NMR spectra (Fig. 3(c)). A shoulder at ∼965 cm^{-1} in the FT-IR spectrum is indicative of $AlVO_4$ [25,26]. These spectra also confirm the dispersion of crystalline VO_x species through the development of the band at 1057 cm^{-1} in the V=O stretching region. Considering the ^{27}Al MAS NMR spectrum of 8 V after calcination, the additional peak at −9 ppm clearly present can, by comparison with the spectrum of the pure material [24], be assigned to $AlVO_4$. Additionally, ^{27}Al MAS NMR studies (Fig. 3(c)) reveal that after calcination the amount of 5-co-ordinate Al detected in 8 V increases considerably, from ∼1% to ∼10% as a result of $AlVO_4$ formation. The formation of $AlVO_4$ through the interaction of VO_x species and alumina under oxidising conditions at the temperatures employed herein is well known [21,22,24,27–32]: however it is dependent upon vanadium loading with high loadings promoting $AlVO_4$ formation [22,27]. Steinfeldt et al. [22] have previously studied the calcination of γ-alumina-supported vanadium catalysts and noted $AlVO_4$ formation only at metal loadings above 4.5 wt.%. Also in agreement with the present study, Steinfeldt et al. observed that at calcination temperatures above 873 K crystalline vanadia species were transformed into smaller polymeric clusters. In the present work, Raman spectroscopy of 8 V after reaction reveals a greater dispersion of VO_x species than in the as-prepared catalysts. This may be due to the dispersion of such species during the calcination procedure.

Considering the influence of calcination on hydroxyl groups, FT-IR studies, Fig. 1(b–d), show that upon calcination of catalyst at 973 K and re-exposure to atmosphere, both basic and acidic OH groups remain on the surface, however the quantity of chemisorbed water is reduced. While some rehydroxylation of the surface will occur upon exposure to atmosphere it should be noted that a recent IR study has revealed that θ-Al_2O_3 does not fully dehydroxylate below 1200 K [33].

3.3. Hydrogen and hydrocarbon reducing environments

The catalytically active species for *n*-butane dehydrogenation are believed to be reduced VO_x species [7,9,16]. Such reduced species may be formed either by pre-reduction of the catalysts in H_2, investigated herein by TEOM, or through *in situ* reduction by the hydrocarbon during reaction, investigated herein by FT-IR, NMR and EPR spectroscopies. These studies demonstrate that reduction effects changes in both VO_x and Al_2O_3 species, with vanadium being reduced from V^{5+} to V^{3+}, and Al_2O_3 undergoing a phase transformation towards a more crystalline material.

The TEOM provides an *in situ* measurement of mass change as a function of time-on-stream, and therefore allows for the redox behaviour of materials to be followed as such processes involve mass changes due to the addition/removal of oxygen. Barteau and co-workers have previously employed TEOM to study such process in VPO catalysts [34–37]. In this work we have studied the interaction of 1 V, 3.5 V, 8 V and the pure support, previously calcined *in situ* at 723 K, with 100% H_2 (50 cm^3 min^{-1}, 0.1 barg) over 2 h at 673 K. This allows mass loss from the catalysts, including the loss of oxygen from VO_x species, to be followed quantitatively with time; the results of this are shown in Fig. 4(a). As can be seen, mass loss is directly related to VO_x loading. For instance after 2 h 8 V has lost 37.7 $\mu g/mg_{cat}$ while 1 V only 24.3 $\mu g/mg_{cat}$. The reduction of VO_x species is not the only source of mass loss from the catalysts, as indicated by the significant mass loss from the pure support. Approximately the same mass loss from the pure support is observed under reducing conditions in complementary TGA-H_2 studies, and is assigned to the desorption of water [9]. Additionally LeBars et al. have suggested that oxygen can be lost from alumina in VO_x/Al_2O_3 catalysts in reducing atmospheres at 823 K [38]. LeBars et al. calculated a loss of 4% of lattice oxygen atoms from the support for VO_x/γ-Al_2O_3 catalyst. Applying the same calculation to the present work yields a value of 4.8%. Regardless of the source of the mass loss from alumina its effects need to be taken into account when considering the reduction of VO_x/Al_2O_3 catalysts. As an approximation one can assume that the support loses the same quantity of material per unit mass with or without vanadium present. The number of

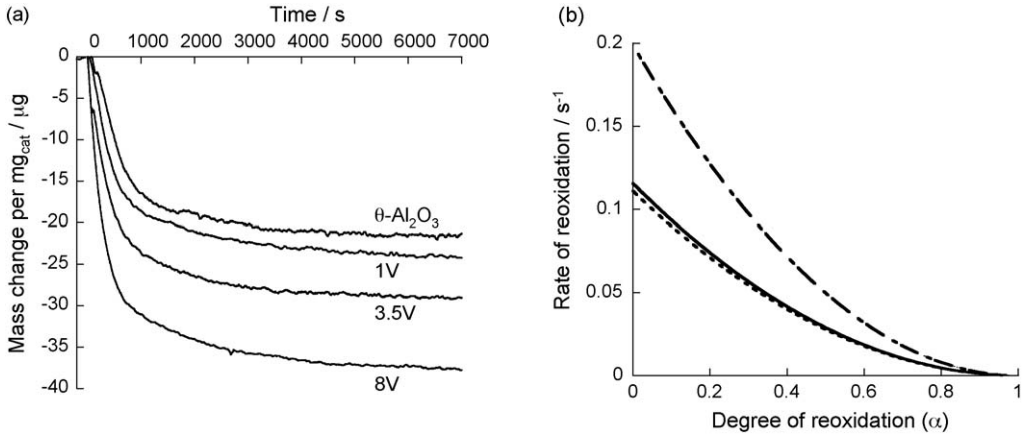

Fig. 4. TEOM data. (a) Mass loss from VO_x/Al_2O_3 during reduction at 673 K. From top: θ-Al_2O_3, 1 V, 3.5 V and 8 V. (b) Rate of reoxidation at 723 K of 1 V (—), 3.5 V (- - -) and 8 V (- – -) as a function of α.

Table 2
Reduction of VO_x/Al_2O_3

Catalyst (V)	Mass loss (O/V)	Oxidation state
1	1.2	2.6
3.5	0.79	3.4
8	0.76	3.5

Calculated mass loss and oxidation state for 1 V, 3.5 V and 8 V reduced in H_2 at 673 K in TEOM studies.

oxygen atoms lost per unit vanadium can then be calculated (Table 2) and these data converted into a vanadium oxidation state as that in the as-prepared catalyst is known to be 5+ [9]. The overall trend of reduction is seen to be towards the formation of V^{3+}. That the higher loading catalysts apparently show a lesser degree of reduction than 1 V may be a consequence of the assumption that the catalysts all lose the same mass from the support. As a result, the oxidation state calculated for catalysts with lower surface areas will be artificially high. Despite this caveat, UV–vis DRS measurements during TGA-H_2 studies reveal the same trend as these TEOM data with mass loss, in oxygen atoms per vanadium, of 1.0 for 1 V and 0.8 for 8 V [9]. As an approximation all three catalyst can be assumed to show a reduction in vanadium oxidation state from 5+ to 3+, in agreement with the literature data [15,39,40].

Despite the apparent reduction of V^{5+} to V^{3+}, previous UV–vis DRS studies have clearly demonstrated the presence of partially reduced V^{4+} species after reduction in H_2 [9]. V^{4+} species are also observed in the present study by EPR spectroscopy after reduction of VO_x during the *n*-butane dehydrogenation reaction. EPR spectra revealed features around $g \sim 2$ indicative of the presence of an axial V^{4+} ion with evidence of partially resolved hyperfine coupling to ^{51}V. Furthermore, peaks to lower field (~2700 G) and an additional half-field feature around 1450 G imply the presence of lower oxidation state V species such as V^{3+} [41]. In contrast to EPR spectroscopy, diffuse reflectance FT-IR spectroscopy did not yield satisfactory results as the dark colour of the catalysts, resulting from both coke deposition and VO_x reduction, resulted in very high absorption. Additionally, after reaction no ^{51}V MAS NMR spectrum was observable. The loss of a signal corresponding to ^{51}V can be assigned to the formation of paramagnetic reduced vanadium species such as V^{3+} and V^{4+}, which are themselves unobservable and, under certain structural conditions, prevent the observation of V^{5+}. This is due to the dipole interaction between the magnetic moments of the V^{5+} nuclei and the paramagnetic nuclei causing the spectral lines to be broadened, often beyond detection [23,42,43].

^{27}Al MAS NMR spectra do not suffer from the same loss of signal as ^{51}V MAS NMR spectra after butane dehydrogenation. Reaction is however observed to have a surprising effect on the nature of the spectra observed. In particular, at higher reaction temperatures, the shape of the peaks changes significantly. For instance, considering the ^{27}Al MAS spectrum of 8 V after reaction at 973 K (not shown) the observed peaks can no longer be approximated by pseudo-Voigt lineshapes but instead are characteristic of a powder pattern [44]. Furthermore, the 5-co-ordinate Al present prior to reduction has been lost. 3.5 V undergoes a similar structural transformation, however 1 V and the pure support do not. At lower reaction temperatures, such as 823 K (the temperature employed in catalytic activity studies, Section 3.4) these changes either do not occur or are much less pronounced. We propose that the origin of the observed changes is a vanadium catalysed phase change of the support towards a more crystalline form. Further support for this hypothesis is provided by surface area measurements, discussed in Section 3.4. A similar phase-change has previously been observed for a 7 wt.% V/γ-Al_2O_3 employed in the dehydrogenation of propane at 873 K [45]. The influence of vanadium species on the crystallinity of alumina supports has also been probed by El-Shobaky et al. [27] and Said [30]. In non-catalytic systems, vanadium-doped γ-Al_2O_3 undergoes phase transformations at lower temperatures than pure γ-Al_2O_3 [46,47]. This may be caused by the dissolution of vanadium into the alumina.

3.4. Relationship to catalytic behaviour

The activity of 1 V, 3.5 V and 8 V towards butane dehydrogenation has been evaluated, in order to determine the surface species responsible for the different reactions occurring during the catalytic process. The main reactions occurring are the formation of retained carbon and the formation of butenes and butadienes. Fig. 5(a) shows the observed conversion and selectivity towards 1-butene and 1,3-butadiene for the three catalysts. In combination with catalyst characterisation data, these data suggest that more isolated VO_x species show the greatest activity towards coke formation while polymeric VO_x are the most active in the dehydrogenation reaction.

While, at 57%, the conversion obtained over 1 V appears high as compared to the other catalysts, this is not a positive attribute as the selectivity towards C_4 dehydrogenation products is very low; 12.7% for 1-butene and 8.1% for 1,3-butadiene. The principle reason for these low values is the high selectivities to retained carbon. Fig. 6 shows ^{13}C CP-MAS spectra of the reacted catalysts.

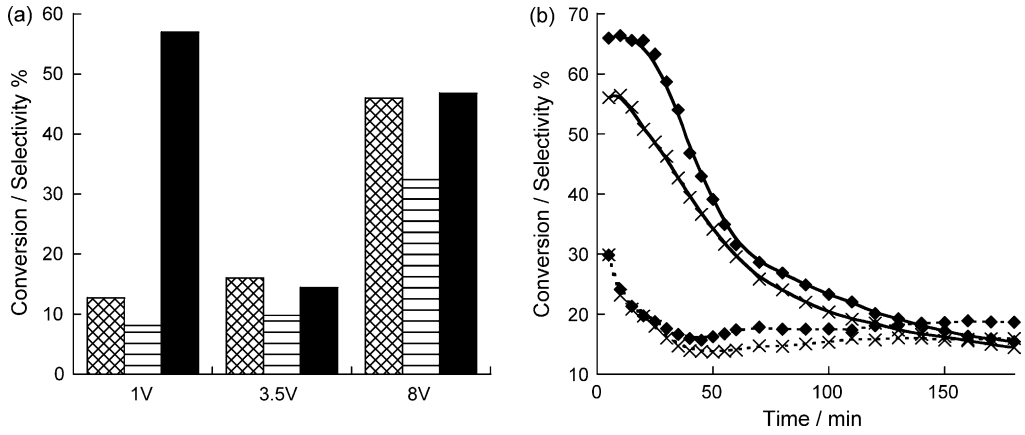

Fig. 5. (a) Selectivity to 1-butene (hatched bars) and 1,3-butadiene (lined bars) and *n*-butane conversion (solid bars) observed over 1 V, 3.5 V and 8 V at 823 K after 180 min on stream. (b) Conversion (solid line) and 1-butene selectivity (dashed line) at 873 K for 3.5 V calcined at 823 K (×) and 973 K (◆).

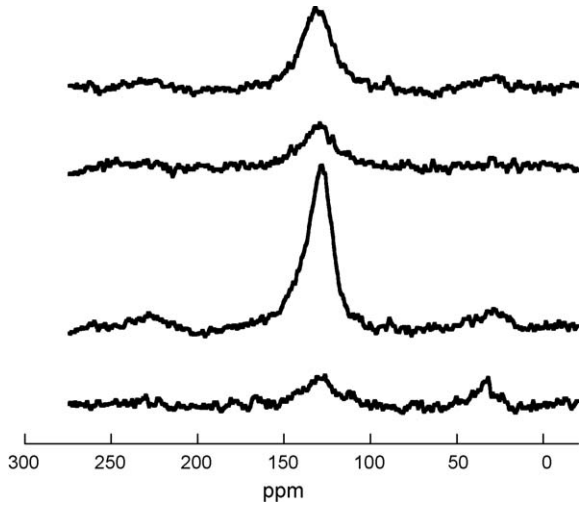

Fig. 6. ^{13}C CP-MAS NMR spectra of VO_x/Al_2O_3 after reaction. From top, 8 V, 3.5 V, 1 V and θ-Al_2O_3.

The large central peak is indicative of carbon in polyolefinic or polynuclear aromatic environments. Elemental microanalysis, shown in Table 3, confirms that the area under the NMR peaks is directly proportional to the amount of coke deposited. It is also possible that some combustion products are formed through interaction with lattice oxygen which are not detected by the FID. In contrast to ODH reactions however, the quantity of such material produced in the direct dehydrogenation of *n*-butane will be very low, as only a very small quantity of oxygen is available for this reaction. This is the case is confirmed through comparison of the elemental microanalysis data (Table 3) and the catalytic activity data (Fig. 5) which indicate that all of the converted *n*-butane can be accounted for through the formation of hydrocarbons and deposited coke. CP-MAS NMR and elemental microanalysis both indicate that 1 V forms very much more coke than either 3.5 V or 8 V despite its lower vanadium loading. This suggests that the more isolated species present on the surface of 1 V are much more efficient at forming carbonaceous material than polymeric and crystalline VO_x species. Previous studies of coke formation on these catalysts by Raman spectroscopy have also observed a far higher selectivity to carbon formation for isolated VO_x than for more polymerised vanadia species [7,9]. While more isolated species show the greatest activity towards carbon formation the data shown in Fig. 5(a) suggest that polymeric vanadia species show the greatest activity in the dehydrogenation reaction. As the quantity of such species increase (1 V < 3.5 V < 8 V) so does the selectivity towards butenes and butadienes. Further evidence that polymeric species are the most active is provided by studies on 3.5 V calcined at two different temperatures, 823 K and 973 K, prior to reaction at 873 K. High temperature calcination has been shown to increase the quantity of polymeric species through dispersion of more crystalline vanadia (Section 3.2). Fig. 5(b) shows that the catalyst calcined at 973 K provides a higher conversion of *n*-butane, particularly in the early stages of reaction where a value of 63% is observed after 25 min, compared to only 49% for the catalyst calcined at the lower temperature. Selectivity towards 1-butene is also improved. These results show good agreement with the previous conclusions of Jackson et al. [8,9]. It should be noted that in contrast to the work of Jackson et al. the present study employs a lower space velocity (~1400 h^{-1}), resulting in a higher selectivity towards butadienes.

Table 3
Weight percent carbon on VO_x/Al_2O_3 after reaction, as detected by elemental microanalysis

Catalyst	wt.% C
θ-Al_2O_3	0.95
1 V	6.68
3.5 V	2.25
8 V	3.59

Table 4
Reoxidation of VO_x/Al_2O_3

Catalyst (V)	Fraction of oxygen replaced (%)	Initial rate of reoxidation (s^{-1})
1	71	0.12
3.5	82	0.11
8	83	0.20

Fraction of oxygen lost during reduction replaced, and the initial rate of reoxidation at 723 K as determined by TEOM.

3.5. Catalyst oxidation and regeneration

The reoxidation of catalysts reduced in H_2 (Section 3.3) and the regeneration of reacted catalysts (Section 3.4) has been investigated. Data on the extent and rate of reoxidation is provided by TEOM, while solid-state NMR, FT-IR, and BET surface area measurements reveal structural changes in the regenerated catalysts compared to the as-prepared samples.

In TEOM studies the reduced catalysts were reoxidised using 100% O_2 (50 cm^3 min^{-1}, 0.1 barg) at 723 K. Table 4 shows the fraction of oxygen replaced as $t \rightarrow \infty$ and the initial rate of this reoxidation process. These values are calculated from Eqs. (3) and (4), respectively; analyses previously applied to the reoxidation of VO_x/TiO_2 catalysts by Słoczynski et al. [15].

$$\frac{t}{\Delta m} = \frac{1}{k(\Delta m)_\infty} + \frac{t}{(\Delta m)_\infty} \quad (3)$$

$$r = \frac{d\alpha}{dt} = k(1-\alpha)^2 \quad (4)$$

Δm represents the mass increase at time t, while α is the degree of reoxidation, *i.e.* $\Delta m/(\Delta m)_\infty$, and k is the rate constant of the process. It is clear from Table 4 that reoxidation does not replace 100% of the oxygen removed during reduction, with lower loading catalysts taking up less oxygen, *e.g.* 1 V replaces 71% of the lost oxygen compared to 83% for 8 V. The rate of reoxidation is also slower for lower loading catalysts. Fig. 4(b) shows this rate as a function of the degree of reoxidation for three catalysts. It is clear that 8 V reoxidises at faster rate than either 1 V or 3.5 V; the initial rate of reoxidation being ~0.2 s^{-1}, as compared to 0.1 s^{-1} for 1 V and 3.5 V. It therefore appears that larger clusters of vanadia units are easier to reoxidise than smaller polymeric or monomeric units. That less oxygen is required for regeneration than was removed during reduction can be explained if larger aggregates of vanadium were to exist on the reoxidised catalysts than on the as-prepared materials as larger clusters have lower O/V ratios; 4:1 for monomeric vanadates, 7:2 for dimers and 5:2 for V_2O_5. The observation that lower loading catalysts reoxidise to a lesser degree has also previously been noted by UV–vis DRS studies [9].

A change in the structure of regenerated catalysts is confirmed through investigation by a variety of techniques. These changes affect both the supported vanadia species and the Al_2O_3 support. Changes in the structure of the VO_x units are observed through ^{51}V MAS NMR and FT-IR spectroscopies. After reaction the catalysts do not yield an observable ^{51}V MAS NMR signal, however regeneration results in the restoration of a spectrum due the oxidation of

paramagnetic V^{3+} and V^{4+} into V^{5+} species. As Fig. 2(d) shows, the spectrum of the regenerated catalyst (in this case 8 V) differs from that of the as-prepared catalyst. The principle difference between the two is that the broad hump, corresponding to disordered V^{5+}, is much reduced in the spectrum of the regenerated catalyst and the intensity of the V_2O_5 peak (δ = −612 ppm) is significantly increased. The spectrum of the regenerated catalyst bears a close resemblance to that of pure V_2O_5 [48]. This confirms that the vanadium present is in a much more ordered, crystalline, environment than it was prior to reaction. Considering the V=O stretching region in IR spectra (Fig. 1(b)–(d)) it is noted that peaks to high wavenumber are reduced in size while those at lower wavenumber are increased, such that the spectrum of 8 V after regeneration is dominated by a band at 1005 cm^{-1}. Similar, but less pronounced, changes are also noted for 3.5 V and 1 V. Comparison with the other data in this work suggests that these changes correspond to the formation of more crystalline VO_x species. Studies on regenerated catalysts therefore support the conclusions from TEOM studies that larger clusters of vanadia are present after reoxidation. These changes alter the catalytic behaviour of the regenerated catalysts with respect to that of the as-prepared materials, as discussed below. For instance, the loss of polymeric VO_x species through the formation of more crystalline species results in reduced *n*-butane conversion as crystalline VO_x have a lower catalytic activity than polymeric species (Section 3.4).

Changes in the nature of the support are observed by ^{27}Al NMR, FT-IR and BET surface area studies. Table 1 shows that the regenerated catalysts have reduced surface area as compared to the as-prepared materials. 1 V has lost only 5% of its surface area, however that of 8 V has reduced by 58% in line with the observed crystallisation of both VO_x species and of the support (Section 3.4). This loss of surface area also results in a reduction in the amount of chemisorbed water as observed by FT-IR (Fig. 1(b)–(d)). Additionally, both ^{27}Al MAS NMR and ^{27}Al 3Q-MAS NMR techniques have been employed to study 8 V regenerated at 873 K. The ^{27}Al 3Q-MAS NMR spectrum (Fig. 3(d)) shows only two resonances in the isotropic projection, at 9.8 ppm and 79.8 ppm, indicating that regeneration has not restored the 5-co-ordinate Al lost under reaction conditions and has not therefore recovered the initial state of the alumina. This is further confirmed by ^{27}Al MAS studies which show a similar powder pattern spectrum to the sample after reaction. Furthermore, regeneration is not observed to result in the appearance of a peak at −9 ppm suggesting that $AlVO_4$ was not formed at this temperature.

These structural changes to the VO_x/Al_2O_3 catalysts after regeneration result in changes in their catalytic behaviour. Jackson and Rugmini have studied these catalysts during multiple *n*-butane dehydrogenation reaction cycles [9]. It was observed that the catalyst activity differed in the second and subsequent cycles from that seen in the first, *e.g.* after 15 min on stream *n*-butane conversion over 3.5 V was 32.9% and 19.1% for the as-prepared and regenerated catalysts, respectively. That this was due to a change in the nature of the VO_x species after regeneration was confirmed by UV–vis spectroscopy studies. In the present work regeneration of the catalysts has been carried out at 873 K, in order to remove the polynuclear aromatics that have formed during reaction. However, such species are not the primary cause of catalyst deactivation in the *n*-butane dehydrogenation reaction. Recent TPO studies have shown that >75% of the observed catalyst deactivation is due to strongly bound reaction intermediates which can be removed from the surface under mild conditions [9].

4. Conclusions

Through the application of a number of analytical techniques we have provided additional insight as to the relationship between surface VO_x species and catalytic activity towards *n*-butane dehydrogenation. Isolated vanadia species show high activity, but very low selectivity due to the undesirable formation of coke. Polymeric VO_x species however show a greater selectivity towards the desired C_4 dehydrogenation products. The formation of polymeric vanadates from V_2O_5-like surface species can be achieved through treatment with O_2 at high temperatures, thereby increasing catalytic activity. After regeneration, the catalytic activity of the catalysts changes as a result of transformations to both the surface VO_x species and the pure support, with vanadium appearing to catalyse a phase transformation in Al_2O_3 above 823 K. The polyolefinic coke species removed by high temperature regeneration are not however the principle source of catalyst deactivation, which can instead be assigned to tightly bound reaction intermediates.

Acknowledgements

Support for this work was provided through the ATHENA project (EPSRC grant GR/R47523/01), funded by EPSRC and Johnson Matthey plc. Dr. Jeremy Rawson (University of Cambridge) is acknowledged for EPR spectroscopy data and Camilla Pepper (University of Cambridge) is thanked for work in acquiring FT-IR spectra.

References

[1] T. Blasco, J.M.L. Nieto, Appl. Catal. A: Gen. 157 (1997) 117.
[2] F. Cavani, N. Ballarini, A. Cericola, Catal. Today 127 (2007) 113.
[3] M.A. Bañares, Catal. Today 51 (1999) 319.
[4] M.V. Martínez-Huerta, X. Gao, H. Tian, I.E. Wachs, J.L.G. Fierro, M.A. Bañares, Catal. Today 118 (2006) 279.
[5] O.R. Evans, A.T. Bell, T.D. Tilley, J. Catal. 226 (2004) 292.
[6] A. Christodoulakis, M. Machli, A.A. Lemonidou, S. Boghosian, J. Catal. 222 (2004) 293.
[7] Z. Wu, P.C. Stair, J. Catal. 237 (2006) 220.
[8] S.D. Jackson, S. Rugmini, P.C. Stair, Z. Wu, Chem. Eng. J. 120 (2006) 127.
[9] S.D. Jackson, S. Rugmini, J. Catal. 251 (2007) 59.
[10] M.E. Harlin, V.M. Niemi, A.O.I. Krause, B.M. Weckhuysen, J. Catal. 203 (2001) 242.
[11] M. Volpe, G. Tonetto, H. de Lasa, Appl. Catal. A: Gen. 272 (2004) 69.
[12] M. Ruitenbeek, A.J. van Dillen, F.M.F. de Groot, I.E. Wachs, J.W. Geus, D.C. Koningsberger, Top. Catal. 10 (2000) 241.
[13] N. Magg, B. Immaraporn, J. Giorgi, T. Schroeder, M. Baumer, J. Dobler, Z. Wu, M. Cherian, E. Kondratenko, M. Baerns, P.C. Stair, J. Sauer, H.J. Freund, J. Catal. 226 (2004) 88.
[14] Z. Wu, H. Kim, P.C. Stair, S. Rugmini, S.D. Jackson, J. Phys. Chem. B 109 (2005) 2793.
[15] J. Słoczynski, R. Grabowski, A. Kozlowska, R. Tokarz-Sobieraj, M. Witko, J. Mol. Catal. A: Chem 277 (2007) 27.
[16] B.M. Weckhuysen, D.E. Keller, Catal. Today 78 (2003) 25.
[17] S.P. Brown, S. Wimperis, J. Magn. Reson. 124 (1997) 279.
[18] D. Chen, E. Bjorgum, K. Christensen, A. Holmen, R. Lodeng, Adv. Catal. 51 (2007) 351.
[19] A.M. Turek, I.E. Wachs, E. DeCanio, J. Phys. Chem. 96 (1992) 5000.
[20] Z. Wu, P.C. Stair, S. Rugmini, S.D. Jackson, J. Phys. Chem. C 111 (2007) 16460.
[21] J.M. Kanervo, M.E. Harlin, A.O.I. Krause, M.A. Banares, Catal. Today 78 (2003) 171.
[22] N. Steinfeldt, D. Muller, H. Berndt, Appl. Catal. A: Gen. 272 (2004) 201.
[23] O.B. Lapina, A.A. Shubin, A.V. Nosov, E. Bosch, J. Spengler, H. Knozinger, J. Phys. Chem. B 103 (1999) 7599.
[24] U.G. Nielsen, A. Boisen, M. Brorson, C.J.H. Jacobsen, H.J. Jakobsen, J. Skibsted, Inorg. Chem. 41 (2002) 6432.
[25] B. Leyer, H. Schmelz, H. Gobel, H. Meixner, T. Scherg, H. Knozinger, Thin Solid Films 310 (1997) 228.
[26] V. Brazdova, M.V. Ganduglia-Pirovano, J. Sauer, J. Phys. Chem. B 109 (2005) 394.
[27] G.A. El-Shobaky, T. ElNabarawy, G. Fagal, M. Mokhtar, J. Therm. Anal. 46 (1996) 1473.
[28] M. Elwahab, A. Said, Collect. Czech. Chem. Commun. 59 (1994) 1983.
[29] A.A. Said, J. Mater. Sci. 27 (1992) 5869.
[30] A.A. Said, J. Mater. Sci. 28 (1993) 3523.
[31] N.R. Shiju, M. Anilkumar, S.P. Mirajkar, C.S. Gopinath, B.S. Rao, C.V. Satyanarayana, J. Catal. 230 (2005) 484.
[32] M. Wakamatsu, S. Ishida, N. Takeuchi, T. Hattori, J. Am. Ceram. Soc. 74 (1991) 1308.
[33] Z. Lodziana, N.Y. Topsoe, J.K. Norskov, Nat. Mater. 3 (2004) 289.
[34] D.X. Wang, M.A. Barteau, J. Catal. 197 (2001) 17.
[35] D.X. Wang, M.A. Barteau, Appl. Catal. A: Gen. 223 (2002) 205.
[36] D.X. Wang, H.H. Kung, M.A. Barteau, Appl. Catal. A: Gen. 201 (2000) 203.
[37] D.X. Wang, M.A. Barteau, Catal. Lett. 90 (2003) 7.

[38] J. LeBars, A. Auroux, M. Forissier, J.C. Vedrine, J. Catal. 162 (1996) 250.
[39] I.E. Wachs, S.S. Chan, R.Y. Saleh, J. Catal. 91 (1985) 366.
[40] A. Baiker, B. Handy, J. Nickl, M. Schramlmarth, A. Wokaun, Catal. Lett. 14 (1992) 89.
[41] J.M. Rojo, J.L. Mesa, R. Calvo, L. Lezama, R. Olazcuaga, T. Rojo, J. Mater. Chem. 8 (1998) 1423.
[42] A.A. Shubin, O.B. Lapina, V.M. Bondareva, Chem. Phys. Lett. 302 (1999) 341.
[43] A.A. Shubin, O.B. Lapina, E. Bosch, J. Spengler, H. Knozinger, J. Phys. Chem. B 103 (1999) 3138.
[44] M.J. Duer, Introduction to Solid-state NMR Spectroscopy, Blackwell, Oxford, 2004.
[45] S.D. Jackson, D. Lennon, G. Webb, J. Willis, Cat. Deact. 2001, Proceedings, 2001, p. 271.
[46] G.C. Bye, D.G. Gavin, J. Am. Ceram. Soc. 57 (1974) 55.
[47] R.A. Shelleman, G.L. Messing, J. Am. Ceram. Soc. 71 (1988) 317.
[48] A.A. Shubin, O.B. Lapina, D. Courcot, Catal. Today 56 (2000) 379.